Cross-Linked Networks of Stiff Filaments Exhibit Negative Normal Stress

Enrico Conti and Fred C. MacKintosh*

Division of Physics and Astronomy, Vrije Universiteit, 1081 HV Amsterdam, The Netherlands

(Received 15 July 2008; published 26 February 2009)

Motivated by recent experiments showing that a variety of stiff biopolymer gels exhibit highly unusual negative normal elastic stresses, we simulate networks of elastic rods over a wide range of concentrations and bending stiffness. In all cases, we find that sheared networks develop significant negative normal stresses that coincide with other elastic nonlinearities, including shear stiffening and compressive bucking. The threshold strain for normal stress in these athermal networks increases with both concentration and stiffness, in contrast with prior predictions for thermal networks. This may provide an experimental test for entropic vs enthalpic effects in such networks.

DOI: 10.1103/PhysRevLett.102.088102 PACS numbers: 87.16.Ka, 62.20.−x, 83.10.−y, 83.60.Df

Networks of semiflexible polymers such as those that make up the cytoskeleton of plant and animal cells have been shown to have rich mechanical and rheological properties. One of the hallmarks of their mechanics is a highly nonlinear elastic response to stress and strain [1–6], including dramatic stiffening under shear. A striking example of such nonlinearity has been the recent demonstration in such systems of highly unusual negative normal stresses—e.g., in which a sample will tend to contract along an axis perpendicular to the direction of shear [7]. Normal stresses, in general, are a nonlinear phenomenon, since their sign cannot depend on the direction of shear, for symmetry reasons. But most materials tend to expand when sheared, as has been known at least since the classic experiments of Poynting 100 years ago [8], in which he showed that elastic rods extend axially when twisted. Another familiar example of this is the tendency of granular materials to dilate when sheared, as can be seen by the fact that wet sand tends to dry out around our feet when we walk on the beach. Few materials have been found to develop negative normal stresses. Liquid crystalline polymers [9], nanotubes [10], and emulsions [11] are examples of such systems, which show rather weakly negative normal stresses in a range of applied shear rates. By contrast, semiflexible polymer networks exhibit negative normal stresses that can become comparable in magnitude to the applied shear stress. Interestingly, this is observed in the *elastic* response of such networks.

It was previously shown theoretically that thermal effects can lead to negative normal stress (NNS) effects due to the asymmetric force-extension relation of semiflexible polymers [7]. Simulations also recently showed large NNS in an athermal network of elastic rods [12], suggesting that purely mechanical effects can also lead to NNS. Here we simulate networks of stiff rods over a wide range of network concentration and polymer stiffness. We find that such athermal networks very generally exhibit NNS that can be comparable to or larger than the corresponding shear stresses, depending on network structure and the strain applied. Although both entropic and enthalpic networks can exhibit NNS, their predicted dependence on both network density and filament stiffness are opposite, providing a possible experimental way to distinguish the importance of entropic vs enthalpic effects.

We construct model networks as follows. A number of straight filaments of length L and random orientation are deposited on a $W \times W$ square. Every time two filaments cross, they are linked together by a free hinge. Filaments that cross the upper or lower boundary are rigidly attached to the boundary and dangling ends are removed, while periodic boundary conditions are applied to the left and right edges of the square. The deposition stops when the desired concentration is reached. We characterize this concentration by the ratio L/ℓ_c, where ℓ_c is the average distance between cross-links along a filament. The network is refined by adding midpoints between cross-links along each filament. Using an energy functional depending on both cross-links and midpoints, we implement a discrete wormlike chain approximation for every filament. For any consecutive pair of points, we consider the stretching energy $\delta\mathcal{H}_{\text{stretch}}$ as a function of the distance ℓ and the initial distance ℓ_0 via a stretching stiffness μ:

$$\delta\mathcal{H}_{\text{stretch}} = \frac{\mu}{2}\left(\frac{\delta\ell}{\ell_0}\right)^2 \ell_0. \tag{1}$$

The bending energy is evaluated for every pair of consecutive segments along a filament:

$$\delta\mathcal{H}_{\text{bend}} = \frac{\kappa}{2}\left(\frac{\delta\theta}{\ell'}\right)^2 \ell', \tag{2}$$

where $\delta\theta$ is the angular deflection of one segment relative to the other, ℓ' is the average length of the two segments, and κ is the bending stiffness. The total energy is the sum of these energies over the entire network. Network shear is performed by displacing the upper boundary with respect to the lower one, followed by a minimization of the elastic energy over the unconstrained internal coordinates (cross-links and midpoints) using a nonlinear conjugate gradient

technique [13]. The resulting shear (normal) stresses are then determined from the forces parallel (perpendicular) to the displaced boundaries.

We simulated networks of size $W = 7$ of filaments with length $L = 1, 2$ and different network densities in the range $L/\ell_c = 9$–60. The bending rigidity κ is varied between 10^{-7} and 10^{-2} keeping a constant $\mu = 1$. For an elastic rod, $\ell_b = \sqrt{\kappa/\mu}$ is a length of order the rod diameter [14]. Thus, the lower limit of our parameter range corresponds to a dimensionless ratio $\kappa/(\mu L^2)$ expected for protein biopolymers with $\ell_b \sim 5$–10 nm and length $L \sim 10$ μm. Our larger values of κ correspond either to shorter filaments or to thermal systems, where the effective modulus μ is greatly reduced by thermal fluctuations [15]. A typical network with $L/\ell_c = 15$ is shown in Fig. 1. Under a purely affine shear, the filaments initially oriented near 45° to the strain direction are stretched (indicated in red) and aligned, while those oriented near 135° are compressed (blue) and eventually buckle. At the filament scale, buckling occurs on wavelengths shorter than L due to the connectivity with the surrounding network through the cross-links, in contrast to classical Euler buckling at the fundamental mode [14].

In Fig. 2 are shown the normal and shear stresses σ_N and σ_S, respectively, for a single network ($L/\ell_c = 13$) in response to an imposed strain γ for various bending stiffnesses κ. The shear response initially depends linearly on strain and eventually stiffens weakly, while the normal response is negative (the network wants to contract) and depends initially quadratically on strain. For an ensemble-averaged network with isotropically oriented filaments, the normal response must, by symmetry, be an even function of the shear deformation. Finite size effects, however, result in a small violation of this for any specific network studied. The shear stress increases with increasing κ, while the magnitude of the normal component exhibits the opposite trend. This behavior is qualitatively consistent with the previous suggestion that the normal stresses arise from the asymmetry of the extensional response of single filaments [7], since stiffer filaments are expected to bend less [15,16] and the energy in Eq. (1) is symmetric. Increased bending and eventual buckling lead to an increasingly asymmetric extensional response, with softening under compression [12].

In Fig. 3(a), we plot the shear modulus $G = \sigma_S/\gamma$ and differential shear modulus $K = d\sigma_S/d\gamma$ normalized by the affine linear modulus $G_{\mathrm{AFF}} = \frac{\pi}{16}\frac{\mu}{L}(\frac{L}{\ell_c} + 2\frac{\ell_c}{L} - 3)$, which corresponds to purely compression or extension deformation without bending filaments [15]. This represents an upper bound for G and K at small strains, since bending modes can only lower the energy for given boundary conditions. For these small strains, a linear regime with constant $K = G = G_0$ is seen in all cases, while nonlinearities such as stiffening and/or softening occur at higher strains. The linear modulus G_0 increases with both density and bending stiffness in agreement with previous work [15–17]. Specifically, $G_0 \propto \kappa$ for floppy filaments, while G_0 saturates to G_{AFF} for stiff filaments (inset) or high densities.

In Fig. 4, we directly compare the shear and normal stresses, by plotting σ_N vs σ_S, both of which have been normalized by G_{AFF}. For stiffer filaments we see an approximate quadratic dependence, which is to be expected by symmetry: Since σ_N must be an even function of strain, it is thus expected to have an initial quadratic dependence for small strain, where σ_S is expected to be approximately linear in strain. Interestingly, for more flexible filaments, this quadratic regime, though present, shrinks and an approximately linear dependence ($-\sigma_N \simeq \sigma_S \sim \gamma$) is observed above a small threshold strain, where the two stresses are of comparable magnitude. A regime with comparable magnitude shear and normal stress was reported for a simulated network in Ref. [12], but the expected small-strain regime with quadratic NNS dependence was not apparent. The crossover we observe from quadratic to linear NNS with strain is consistent with what was found experimentally and theoretically in Ref. [7]. This behavior can be understood in simple terms

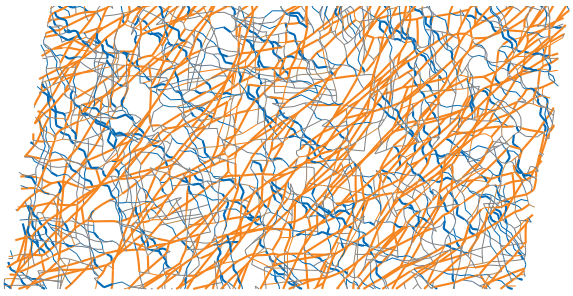

FIG. 1 (color online). A portion of a typical network for $\gamma \simeq 0.16$. Red indicates stretched segments, while blue indicates compressed ones. Filaments oriented near 45° are stretched, and those near 135° are compressed.

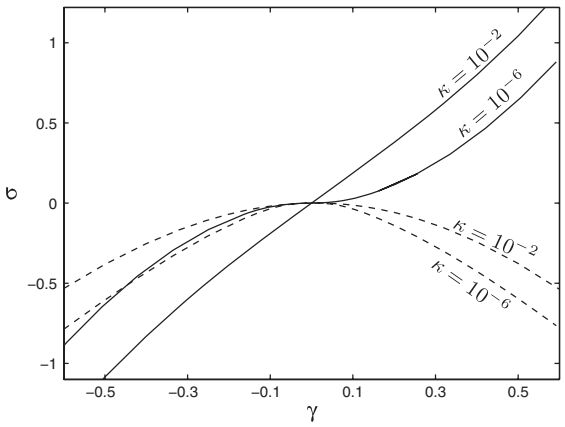

FIG. 2. Raw shear (solid line) and normal (dashed line) stresses vs strain for different bending stiffnesses.

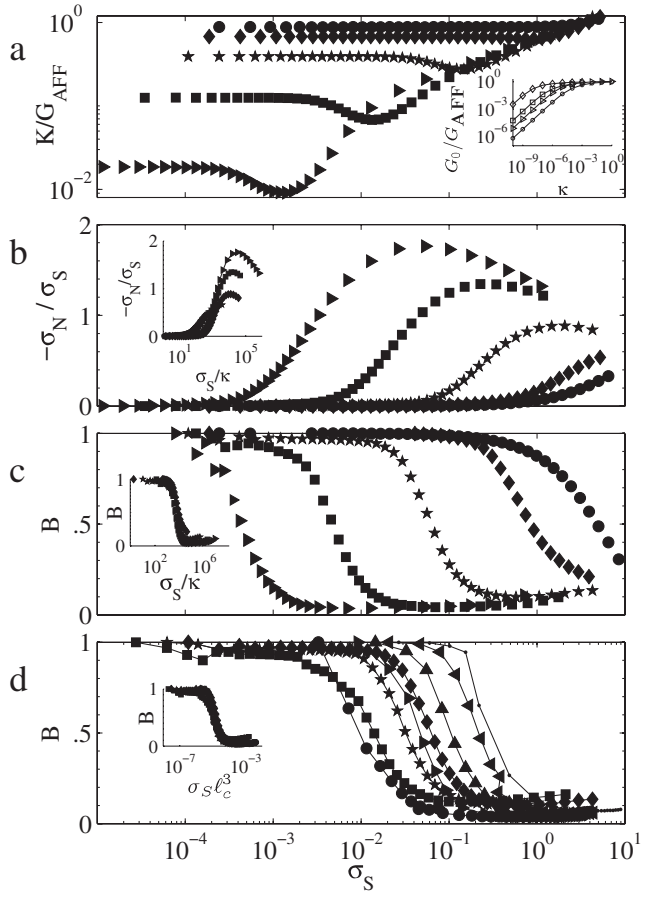

FIG. 3. In (a), (b), and (c), the differential shear modulus K normalized by G_{AFF}, the ratio of normal to shear stress, and the buckling order parameter B, respectively, are all plotted vs shear stress for constant density $L/\ell_c = 15$ and for various bending stiffnesses $\kappa = 10^{-7}$ (▶), $\kappa = 10^{-6}$ (■), $\kappa = 10^{-5}$ (★), $\kappa = 10^{-4}$ (◆), and $\kappa = 10^{-3}$ (●). In the inset of (a), the ratio G_0/G_{AFF} is plotted vs the bending stiffness κ for different densities $L/\ell_c = 9$ (●), 13 (▶), 20 (■), and 40 (◆). Here G_0 grows linearly with κ for soft filaments and saturates to G_{AFF} for stiff ones; G_0/G_{AFF} also increases with density. The insets in (b) and (c) show data collapse for $-\sigma_N/\sigma_S$ and B when plotted against σ_S/κ. In (d), B is plotted for constant $\kappa = 10^{-5}$ and various densities $L/\ell_c = 11$ (★), $L/\ell_c = 13$ (◆), $L/\ell_c = 15$ (●), $L/\ell_c = 20$ (▶), $L/\ell_c = 30$ (▲), $L/\ell_c = 40$ (◀), $L/\ell_c = 50$ (▼), and $L/\ell_c = 60$ (·). The inset in (d) shows the collapse of these data when plotted against $\sigma_S \ell_c^3$. Together with the insets in (b) and (c), this shows that the onset of nonlinearity coincides with the buckling transition.

for highly asymmetric extensional response of filaments, in which both σ_S and σ_N are dominated by the stretched filaments oriented near 45° to the strain direction [7]. Our results suggest that the crossover from quadratic to linear NNS behavior occurs for smaller strains with more flexible filaments, which can be tested experimentally.

To test this more directly, we plot the ratio $-\sigma_N/\sigma_S$ vs γ in Fig. 5. Here we see that the small-strain regime, characterized by $\sigma_N \sim \gamma^2$ and $\sigma_N/\sigma_S \sim \gamma$, decreases with

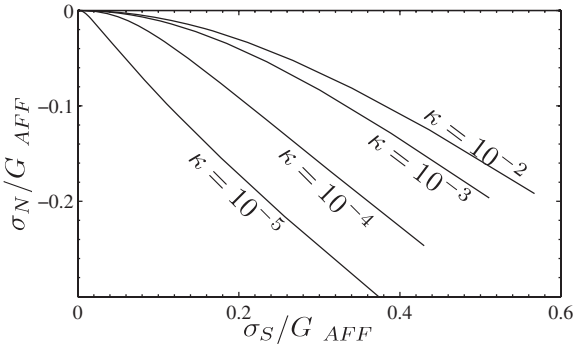

FIG. 4. Normal stress σ_N vs shear stress σ_S (both normalized by G_{AFF}) for density $L/\ell_c = 13$ and various filament bending stiffnesses. For stiff filaments, $\sigma_N \sim \gamma^2 \sim \sigma_S^2$ over a large initial stress region. For softer filaments, this region becomes smaller so that on this linear scale it appears that $\sigma_N \sim \sigma_S$.

increasing flexibility of filaments or decreasing network concentration. Interestingly, this is opposite to the predicted behavior for thermally fluctuating networks in Ref. [7]. Thus, the normal stresses may provide an experimental signature for thermal vs nonthermal systems. We also observe an apparent convergence of all networks for increasing strain, to a regime in which the two stress components are comparable. As the filaments become softer to bending, we observe a peak, with normal stresses exceeding shear stresses for small strains. Reference [7] reported normal stress that exceeded the shear stress in some cases. Subsequent experiments [18] find a peak similar to that of Fig. 5.

As argued in Ref. [7], one possible origin of negative normal stresses can be the asymmetric extensional response or force-extension relation of the constituent fila-

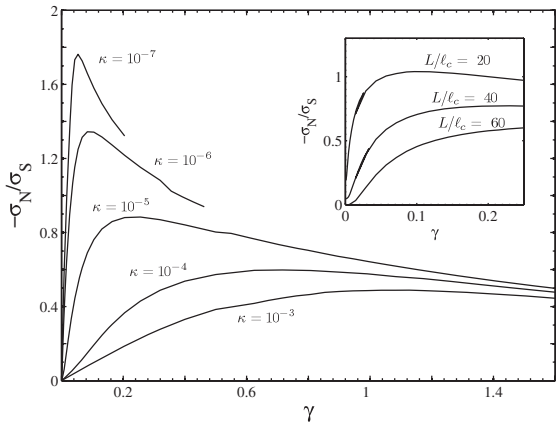

FIG. 5. The ratio of normal to shear stress vs applied strain γ for constant density $L/\ell_c = 15$ and various filament bending stiffnesses. On decreasing κ, a peak grows, becoming more pronounced and moving to smaller strain. For large strain, the curves depend weakly on κ, showing a regime dominated by stretching only. The inset shows the same ratio $-\sigma_N/\sigma_S$ for constant stiffness $\kappa = 10^{-5}$ and different densities.

ments. Even though the individual filaments in our model are assumed to be Hookean springs, with a symmetric force-extension curve, the fact that they can bend and buckle effectively gives rise to a softer response to compression and an asymmetric force-extension relation [12]. To test whether this can explain our results, we measure the relative importance of buckling with an order parameter B defined by $\frac{dE_C}{d\gamma} / \frac{dE_{\mathrm{TOT}}}{d\gamma}$. Here the numerator refers to the incremental change in the elastic compression energy of the filament segments under compression in the network for a small-strain step $d\gamma$, evaluated as a function of the initial state of network strain γ. The denominator refers to the incremental change in total elastic energy. This is normalized by its initial, small-strain value, where no buckling is expected. Thus, this order parameter should have an initial value of unity and should then decrease as filaments begin to buckle because this relieves their compression energy. We plot this in Fig. 3, along with both K/G_{AFF} and $-\sigma_N/\sigma_S$ for several different networks of the same density, but with differing bending stiffness. We see that the onset of significant buckling, indeed, coincides with the onset of nonlinearities in the rheology. Furthermore, classical Euler buckling theory predicts that the threshold force for buckling is proportional to κ. By plotting both B and $-\sigma_N/\sigma_S$ vs σ_S/κ, we see collapse of the curves for various κ (see insets), consistent with the dominant role of buckling in controlling the development of large normal stresses. In Fig. 3(d), we plot B for various L/ℓ_c, and we see that the curves collapse (inset) by plotting against $\sigma_S \ell_c^3$, confirming that the buckling order parameter actually accounts for the collective buckling of inter-cross-link segments [19].

Here we have calculated the component of stress in the shear gradient direction that, as discussed in Ref. [7], is appropriate for normal stress measurements in the elastic limit of low frequency, where the network is expected to be compressible. The NNS in semiflexible networks can be qualitatively understood in terms of the nonlinear and asymmetric force-extension relation, which can result either from thermal effects [7,20] or from Euler buckling of the filaments under compression [12,17]. This can explain, in part, the apparent generality of NNS reported for a number of different stiff biopolymer systems [7], which should span thermal and athermal systems. Furthermore, our results suggest a possible way to distinguish experimentally between alternative thermal [2,3,20] vs athermal [12,17] origins of nonlinear elasticity in biopolymer networks: We find that the characteristic strain for the onset of negative normal stress increases with network concentration and filament stiffness, both of which are in contrast with the prediction for thermal networks [7]. Although we have focused on isotropic networks, anisotropy can also occur *in vivo* or can result from sample preparation *in vitro*. In general, anisotropy is expected to result in shear (normal) stresses that are no longer (anti)symmetric in strain, meaning that both positive and negative normal stress can be expected. Thus, normal stress measurements may provide a good experimental test for isotropy.

We thank C. Broedersz, M. Das, and P. Janmey for useful discussions. This work was supported in part by FOM/NWO.

*fcm@nat.vu.nl

[1] P. A. Janmey *et al.*, J. Cell Biol. **113**, 155 (1991).
[2] M. L. Gardel, J. H. Shin, F. C. MacKintosh, L. Mahadevan, P. Matsudaira, and D. A. Weitz, Science **304**, 1301 (2004).
[3] C. Storm, J. Pastore, F. C. MacKintosh, T. C. Lubensky, and P. A. Janmey, Nature (London) **435**, 191 (2005).
[4] B. Wagner, R. Tharmann, I. Haase, M. Fischer, and A. R. Bausch, Proc. Natl. Acad. Sci. U.S.A. **103**, 13 974 (2006).
[5] K. E. Kasza, A. C. Rowat, J. Liu, T. E. Angelini, C. P. Brangwynne, G. H. Koendelink, and D. A. Weitz, Curr. Opin. Cell Biol. **19**, 101 (2007).
[6] O. Chaudhuri, S. H. Parekh, and D. A. Fletcher, Nature (London) **445**, 295 (2007).
[7] P. A. Janmey *et al.*, Nature Mater. **6**, 48 (2007).
[8] J. H. Poynting, Proc. R. Soc. A **82**, 546 (1909).
[9] G. Marrucci, *Liquid Crystallinity in Polymers: Principles and Fundamental Properties* (VHC Publishers, New York, 1991).
[10] S. Lin-Gibson *et al.*, Phys. Rev. Lett. **92**, 048302 (2004).
[11] A. Montesi, A. A. Peña, and M. Pasquali, Phys. Rev. Lett. **92**, 058303 (2004).
[12] C. Heussinger, B. Schaefer, and E. Frey, Phys. Rev. E **76**, 031906 (2007).
[13] W. H. Press, S. A. Teulosky, W. T. Wetterling, and B. P. Flannery, *Numerical Recipes in C* (Cambridge University Press, Cambridge, England, 1992), 2nd ed.
[14] L. D. Landau and E. M. Lifshitz, *Theory of Elasticity* (Pergamon Press, Oxford 1986), 2nd ed.
[15] D. A. Head, A. J. Levine, and F. C. MacKintosh, Phys. Rev. Lett. **91**, 108102 (2003); Phys. Rev. E **68**, 061907 (2003).
[16] J. Wilhelm and E. Frey, Phys. Rev. Lett. **91**, 108103 (2003).
[17] P. R. Onck, T. Koeman, T. van Dillen, and E. van der Giessen, Phys. Rev. Lett. **95**, 178102 (2005).
[18] H. King *et al.*, J. Phys. Chem. (to be published).
[19] For a rod of length ℓ_c, the buckling force $f_{\mathrm{crit.}} \sim \kappa/\ell_c^2$, for which the macroscopic stress is proportional to $f_{\mathrm{crit.}}$ times the flux of filaments crossing the surface $\sim 1/\ell_c$, from which we obtain $\sigma_S^{\mathrm{crit.}} \sim \kappa/\ell_c^3$.
[20] F. C. MacKintosh, J. Käs, and P. A. Janmey, Phys. Rev. Lett. **75**, 4425 (1995).